Impurity-induced Raman spectra of CsBr:Tl^+: A breathing-shell-model calculation

M. S. Haque,* D. Strauch, H. Krause, and T. Suski†
Fachbereich Physik, Universität Regensburg, D 8400 Regensburg, Federal Republic of Germany
(Received 29 March 1977)

The Raman spectra of CsBr:Tl^+ at 16 K have been measured. The E_g spectrum shows some differences from the one at 300 K. A (breathing) shell model calculation of the spectra has been made and a set of harmonic-perturbation parameters have been obtained which describe the E_g and T_{2g} spectra in good agreement with experiment. The A_{1g} spectrum was too weak to be detected. Inclusion of the polarizability derivatives at the defect's second neighbors resolves a puzzle set up in previous work.

I. INTRODUCTION

In a recent publication,[1] an attempt was made by two of the present authors to obtain a symmetry-independent lattice-dynamical model of the perturbed crystal, CsBr:Tl^+ at 4.2 K, by calculating its defect-induced infrared spectrum using a full breathing-shell-model (BSM) formalism. Polarizability effects were consistently incorporated in these calculations, and the perturbed-crystal model was obtained in terms of perturbed BSM parameters pertaining to the host-crystal phonons.[2] Although the calculated spectrum could be brought into a very good agreement with the observed one,[3] a unique set of parameters could not be determined on account of the necessarily large number of parameters involved in the model and the scarcity of features in the observed spectrum. This uncertainty was two-fold. First, the two parameters describing the polarizability of the defect ion could not be uniquely determined even though a polarizability change was shown to influence the spectrum. Second, the various parameters describing the host-defect coupling and the lattice relaxation were not quite unique. While the first-order defect-induced Raman spectra are independent of the defect polarizability and thus the former parameters will be left uncertain, the latter set of parameters will be pinned down to an as great a degree as possible. This is the aim of the present paper.

As is very well known, first-order Raman spectra are forbidden in pure alkali halides on account of inversion symmetry. Implantation of an impurity into the crystal not only removes this inversion symmetry but also destroys the lattice periodicity, consequently allowing continuous first-order spectra to be observed. Such spectra reflect the perturbed phonon density of states weighted by the amplitudes of motion of the defect's neighboring ions. The spectra, therefore, contain information on the lattice dynamics of the perturbed crystal and can consequently be used to narrow down the choice of perturbed parameters in our model for the perturbed system, CsBr:Tl^+.

The experimental and calculated first-order Raman spectra of thallium-doped Cs halides at room temperature have been published by Buchanan *et al.*[4] Our model for the perturbed crystal is valid at 4.2 K, and therefore, it was necessary to perform a set of measurements at low temperatures. The calculated spectra in Ref. 4 were obtained by using a formal force-constant (rigid-ion) model, and as such the perturbed parameters are not expected to be the same for phonons of different symmetry types (see Ref. 1). We shall demonstrate that the same set of perturbed parameters in our model can be used to calculate the infrared and the Raman spectra.

It was found in Ref. 4 that in order to reproduce the E_g spectrum for CsBr:Tl^+ the change in the transverse force constant between the impurity and its nearest neighbors had to be three times as large as the change in the corresponding longitudinal force constant. Such a result appears to be doubtful, since the transverse force constant in the unperturbed crystal is about an order of magnitude smaller than the longitudinal one.[5] Moreover the calculated E_g spectrum is not in very good agreement with the experimental one. We shall show that this spectrum can be obtained by including the polarizability derivatives on the defect's second neighbors, and that it is unnecessary to assume such unreasonable force-constant changes as was done in Ref. 4.

II. EXPERIMENT

The Raman spectra of CsBr:Tl^+ were measured using a 2-W Ar laser, a 1-m double monochromator and a Channeltron detector with photon-counting equipment. The crystal was placed in a small evaporation cryostat, and the measurements were performed at 16 K for two different geometries corresponding to the E_g and the T_{2g} spectra. As in Ref. 4, the A_{1g} spectrum for CsBr:Tl^+ was too

weak to be observed.

To determine the extent of second-order Raman scattering in the measured spectra of CsBr:Tl^+, the spectra of pure CsBr were also measured. At 16 K, almost no scattering was observable from the pure sample for frequencies below the one-phonon cut-off frequency (~120 cm^{-1}); although this scattering increased very rapidly with increasing temperatures. In view of this fact, we believe that the observed spectra for CsBr:Tl^+ at 16 K, and for frequencies $\lesssim 120$ cm^{-1}, are the first-order defect-induced spectra.

The observed E_g spectrum of CsBr:Tl^+ is shown in panel 1 of Fig. 2, and the corresponding T_{2g} spectrum is presented in panel 1 of Fig. 3. Although the relative intensities of the peaks in the E_g spectrum are different from those of the corresponding room-temperature spectrum,[4] the peak positions in both the E_g and T_{2g} spectra shift up in frequencies by only 6 cm^{-1} or less when the crystal is cooled down from 300 to 16 K. It is therefore doubtful that any further changes in the spectra would be observed between 16 and 4.2 K.

III. THEORY

The Raman scattering tensor for first-order scattering is given by[6]

$$i_{\alpha\beta\gamma\delta}(-\omega)=\pi^{-1}\hbar\eta(\omega)\sum_{\Gamma}\underline{P}_{\alpha\beta}(\Gamma)\,\mathrm{Im}\underline{G}(\Gamma\,|\,\omega)\underline{P}_{\gamma\delta}(\Gamma)\,. \quad (1)$$

Here, ω is the frequency shift, and $\eta(\omega)=1/(1-e^{-\beta\hbar\omega})$. $\mathrm{Im}\underline{G}(\Gamma\,|\,\omega)$ and $\underline{P}_{\alpha\beta}(\Gamma)$ are the imaginary part of the Green's-function matrix and the vector of the first-order electronic polarizability derivatives, respectively. Γ refers to a symmetry basis.

Let $\vec{\xi}_Q(\vec{r}\,|\,\Gamma t)$ be an element of a symmetry basis vector; here, Γ is the representation, t a realization, $\vec{r}$ a lattice point, and Q refers to shell (S) or breathing (B) displacements. These elements are listed in Table I for the defect's first, second, and fourth neighbors, and for the three Raman-active representations A_{1g}, E_g, and T_{2g}. For the E_g and T_{2g} representations, only one partner from each is shown. Note that the T_{2g} representation has two realizations on the first and fourth neighbors, but only one on the second neighbors. For the E_g representation, the fourth neighbors make zero contribution. We have shown in Ref. 1 that the breathing motion on the second and fourth neighbors do not have any significant effect on the spectrum. Consequently, they are left out of the present calculations. In the symmetry basis the elements of $\underline{P}_{\alpha\beta}(\Gamma)$ are given by

$$P_{\alpha\beta}(\Gamma t)=\sum_{\vec{r}Q}\vec{\xi}_Q(\vec{r}\,|\,\Gamma t)\partial P_{\alpha\beta}/\partial\vec{u}_Q(\vec{r})\,; \quad (2)$$

here, $\vec{u}$ is a vibrational displacement of particle Q at site $\vec{r}$. We assume that the polarizability derivatives are nonzero only on the first and second neighbors of the defect. No polarizability derivatives are being associated with the breathing degree of freedom.

Using the basis vectors listed in Table I and the symmetry operations of the group O_h we obtain

TABLE I. Symmetry eigenvectors in the defect subspace for Raman-active modes: Elements of only half of the particles ar $\vec{r}$ are shown, the other half is obtained from $\vec{\xi}_S(\vec{r})=-\vec{\xi}_S(-\vec{r})$; $\xi_B(\vec{r})=\xi_B(-\vec{r})$.

$\vec{r}$	000	111 222	$\bar{1}11$ $\bar{2}\bar{2}2$	$\bar{1}\bar{1}1$ $\bar{2}\bar{2}2$	$1\bar{1}1$ $2\bar{2}2$	200	020	002
$\sqrt{24}\,\vec{\xi}_S(A_{1g},1),\sqrt{24}\,\vec{\xi}_S(A_{1g},5)$	(0,0,0)	(1,1,1)	$(\bar{1},1,1)$	$(\bar{1},\bar{1},1)$	$(1,\bar{1},1)$	(0,0,0)	(0,0,0)	(0,0,0)
$\sqrt{6}\,\vec{\xi}_S(A_{1g},2)$	(0,0,0)	(0,0,0)	(0,0,0)	(0,0,0)	(0,0,0)	(1,0,0)	(0,1,0)	(0,0,1)
$\xi_B(A_{1g},3)$	1	0	0	0	0	0	0	0
$\sqrt{8}\,\xi_B(A_{1g},4)$	0	1	1	1	1	0	0	0
$4\vec{\xi}_S(E_g,1),4\vec{\xi}_S(E_g,3)$	(0,0,0)	$(0,1,\bar{1})$	$(0,1,\bar{1})$	$(0,\bar{1},\bar{1})$	$(0,\bar{1},\bar{1})$	(0,0,0)	(0,0,0)	(0,0,0)
$2\vec{\xi}_S(E_g,2)$	(0,0,0)	(0,0,0)	(0,0,0)	(0,0,0)	(0,0,0)	(0,0,0)	(0,1,0)	$(0,0,\bar{1})$
$\sqrt{8}\,\vec{\xi}_S(T_{2g},1),\sqrt{8}\,\vec{\xi}_S(T_{2g},5)$	(0,0,0)	$(1,0,0)$	$(\bar{1},0,0)$	$(1,0,0)$	$(\bar{1},0,0)$	(0,0,0)	(0,0,0)	(0,0,0)
$4\vec{\xi}_S(T_{2g},2),4\vec{\xi}_S(T_{2g},6)$	(0,0,0)	(0,1,1)	(0,1,1)	$(0,1,\bar{1})$	$(0,0,\bar{1})$	(0,0,0)	(0,0,0)	(0,0,0)
$2\vec{\xi}_S(T_{2g},3)$	(0,0,0)	(0,0,0)	(0,0,0)	(0,0,0)	(0,0,0)	(0,0,0)	(0,0,1)	(0,1,0)
$\sqrt{8}\,\xi_B(T_{2g},4)$	0	1	1	$\bar{1}$	$\bar{1}$	0	0	0

$$\underline{P}(A_{1g}) = \begin{pmatrix} P_{yy}(111,y)+2P_{yy}(111,z) \\ \frac{1}{2}[P_{yy}(020,y)+2P_{yy}(002,z)] \\ 0 \\ 0 \\ 0 \end{pmatrix}, \tag{3a}$$

$$\underline{P}(E_g) = \begin{pmatrix} P_{yy}(111,y)-P_{yy}(111,z) \\ \frac{1}{2}[P_{yy}(020,y)-P_{yy}(002,z)] \\ 0 \end{pmatrix} = \begin{pmatrix} \pi_1 \\ \pi_2 \\ 0 \end{pmatrix}, \tag{3b}$$

and

$$\underline{P}(T_{2g}) = \begin{pmatrix} \sqrt{2}\,P_{yz}(111,x) \\ 2P_{yz}(111,y) \\ P_{yz}(200,z) \\ 0 \\ 0 \\ 0 \end{pmatrix}. \tag{3c}$$

With these the following three independent elements of the Raman scattering tensor are obtained,

$$i_{xxxx} = (8\hbar\eta/3\pi)[I(A_{1g}) + 2I(E_g)], \tag{4a}$$

$$i_{xxyy} = (8\hbar\eta/3\pi)[I(A_{1g}) - I(E_g)], \tag{4b}$$

$$i_{xyxy} = (4\hbar\eta/\pi)I(T_{2g}), \tag{4c}$$

TABLE II. Perturbation matrix in the E_g representation. Symbols are explained in the text.

$$\begin{pmatrix} \delta f_t + \frac{4}{3}\delta f_s + 2\delta f_1 & -\frac{4}{3}\delta f_s \\ -\frac{4}{3}\delta f_s & \delta f_2 + \frac{4}{3}\delta f_s \end{pmatrix}$$

with

$$I(\Gamma_i) = \underline{P}^T(\Gamma_i)\,\mathrm{Im}\underline{G}(\Gamma_i)\underline{P}(\Gamma_i). \tag{5}$$

The perturbed Green's function matrices $\underline{G}(\Gamma_i)$ are computed from the corresponding unperturbed ones and from the perturbation matrices. The same host-crystal phonons[2] for the unperturbed Green's functions and the same defect parameters for the perturbation matrices are used as in Ref. 1.

In Tables II and III, we present the perturbation matrices in the symmetrized E_g and T_{2g} representations, respectively. Since the A_{1g} spectrum in CsBr:Tl⁺ is too weak to be observed, we leave this spectrum out of our calculations. The notation used in Tables II and III is that of Ref. 1. We repeat the meaning of the quantities here for clarity. δf_l and δf_t are the changes in the longitudinal and the transverse shell-shell force constants, respectively, between the defect and its first neighbors; δf_1 is the change in the longitudinal shell-shell force constant among the first neighbors; δf_4 is the change in the longitudinal shell-shell force constant between the first and the fourth neighbors; δf_s is the change in the longitudinal shell-shell force constant between the first and the second neighbors, δf_2 is the change in the longitudinal shell-shell force constant between the defect and the second neighbors. δf_1, δf_4, and δf_s simulate the effect of relaxation of the defect's nearest neighbours and/or the change of electron-

TABLE III. Perturbation matrix in the T_{2g} representation.

$$\begin{pmatrix} \lambda_{11} & \lambda_{12} & -\frac{1}{3}\sqrt{8}\,\delta f_s & -(\delta f_l + \delta f_s)/\sqrt{3} & -\frac{1}{3}\delta f_4 & -\frac{1}{3}\sqrt{2}\,\delta f_4 \\ & \lambda_{22} & 0 & -\sqrt{2}\,(\delta f_t + \delta f_s)/\sqrt{3} & -\sqrt{2}\,\delta f_4/3 & -\frac{2}{3}\delta f_4 \\ & & \frac{4}{3}\delta f_s & \sqrt{8}\,\delta f_s/\sqrt{3} & 0 & 0 \\ & & & \lambda_{44} & -\delta f_4/\sqrt{3} & -\sqrt{2}\,\delta f_4/\sqrt{3} \\ & & & & \delta f_4/3 & \sqrt{2}\,\delta f_4/3 \\ & & & & & \frac{2}{3}\delta f_4 \end{pmatrix}$$

$$\lambda_{11} = \tfrac{1}{3}(\delta f_l + 2\delta f_t) + \delta f_s + 2\delta f_1 + \tfrac{1}{3}\delta f_4,$$
$$\lambda_{12} = \tfrac{\sqrt{2}}{3}(\delta f_l - \delta f_t - \delta f_s + \delta f_4),$$
$$\lambda_{22} = \tfrac{2}{3}(\delta f_l + \tfrac{1}{2}\delta f_t + \delta f_s + \delta f_4),$$
$$\lambda_{44} = \delta f_l + 3\delta f_s + \delta f_1 + \delta f_4.$$

ic eigenstates at these neighbors induced by the defect, while δf_1, δf_t, and δf_2 represent the change in the direct coupling of the defect to the lattice.

IV. RESULTS AND DISCUSSION

As we have already mentioned in Sec. I, the primary aim of this paper is to obtain a lattice-dynamical model for CsBr : Tl^+ which can be used for calculating perturbed phonons of any symmetry type. Hence in order to calculate the first-order Raman spectra of CsBr : Tl^+, the most important criterion that the perturbed BSM parameters (see Tables II and III) must satisfy is that they reproduce the experimental infrared (T_{1u}) spectrum[3] as well.

It was found[1] that the experimental features of the infrared spectrum at higher frequencies cannot be reproduced by the theory without perturbing the motion of the defect's second neighbors. This can be done either by a direct coupling of the defect to its second neighbors, i.e. by δf_2, or by a combination of δf_2 and δf_s. The exact combination of these two parameters cannot be determined uniquely from the infrared spectrum alone because of the lack of sufficient features in it. We will demonstrate to which extent the Raman spectra help to determine the perturbation parameters.

Figure 1 shows the experimental and calculated infrared spectra of CsBr : Tl^+. The calculated spectrum shown in panel 2 is the one which was presented in Ref. 1. The curves shown in panel 2 of Figs. 2 and 3 are calculated with the same set of parameters as used for the curve in panel 2 of Fig. 1. For this set of parameters the best possible E_g spectrum is obtained with a contribution of the second-neighbor polarizability given by $\pi_2/\pi_1 = 1.25$, see Eq. (3b). Even though the T_{2g} spectrum is reproduced very well, the E_g spectrum is not. In order to improve the agreement between the theoretical and experimental E_g spectrum the shell-model parameters must be changed. A set of parameters which yield reasonably good T_{1u}, E_g, and T_{2g} spectra is quoted in panel 3 of Figs. 1–3 where the corresponding spectra are shown. We will comment on some details.

In Fig. 2, we present the low-temperature experimental and calculated E_g spectrum of CsBr : Tl^+. The spectrum drawn with the broken line is obtained from the polarizability derivatives of just the defect's first neighbors ($\pi_2 = 0$) in which case the intensity of the peak at 44 cm^{-1} is much too low. One way to increase the intensity of this peak relative to those of the two neighboring ones at higher frequencies is by using unreasonably large negative values of δf_t as was done by Buchanan *et al.*[4] However, such a value for δf_t totally destroys the calculated infrared spectrum. Another way of obtaining the correct relative intensities is to include nonzero values for the polarizability derivatives on the defect's second neighbors as well; the spectrum drawn with a continuous line has been calculated by using $\pi_2/\pi_1 = 0.75$. Recall that the defect's second neighbors are the heavier Cs^+ ions and that their distance from the defect site is only 15% larger than that of the first neighbors. Hence it is not unreasonable that the large peak in the acoustic region of the spectrum arises from the vibrations of the heavier Cs^+ ions in the second neighboring positions.

The E_g spectrum is independent of the parameters δf_1 and δf_4, and although it is not very sensitive to small changes in δf_s and δf_t, the infrared (T_{1u}) spectrum is. The combination of the T_{1u} and the E_g spectrum determines the parameters δf_s and δf_t to within 20%. We have shown in Ref.

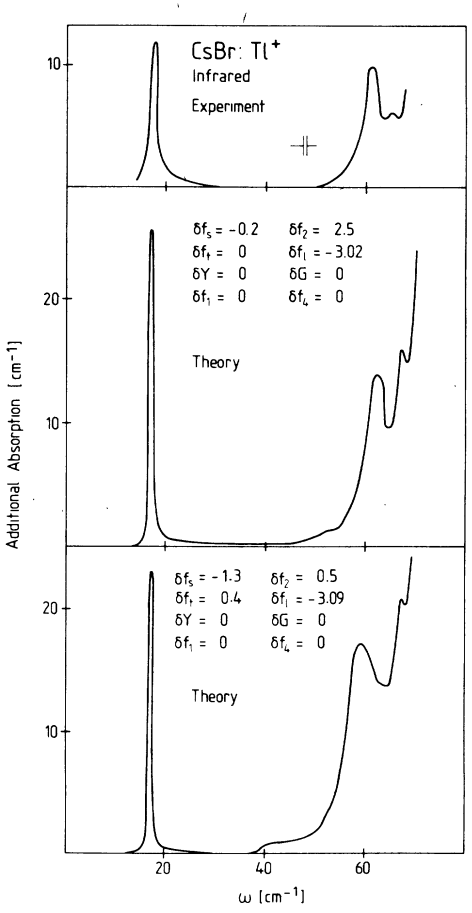

FIG. 1. Experimental and calculated defect-induced infrared spectrum of CsBr:Tl^+. The experimental spectrum, which is shown in panel 1 is taken from Ref. 2, while the calculated spectrum in panel 2 is the one given in Ref. 1.

1 that, due to uncertainties in the calculated and the experimental infrared spectrum near the resonance frequency, one is unable to determine the perturbed parameters δY (shell charge) and δG (core-shell force constant). Moreover, since the Raman-active modes are of even parity, for which the defect remains stationary, δY and δG are not involved in the Raman calculations and consequently remain undetermined. Assuming $\delta Y = \delta G = 0$, the infrared and Raman spectra determine δf_l and δf_t to within 20%. We would like to point out that both δf_l and δf_t depend rather sensitivity on the values of δY and δG, and hence the actual uncertainties in the values of these two parameters are much larger than 20%.

Figure 3 shows the low-temperature experimental and calculated T_{2g} spectra of CsBr:Tl⁺. Recall that for the irreducible representation T_{2g} there are two realizations on the defect's first neighbors. The calculated spectrum corresponds to $G(T_{2g}, 2, 2)$ and is seen to be in good agreement with the experiment. The spectrum obtained from $G(T_{2g}, 1, 1)$ does not correspond to the experiment at all (see also Ref. 3). We have also drawn (broken curve in panel 3) the contribution from $G(T_{2g}, 3, 3)$, which represents the motion of the defect's second neighbors. One can readily see that the latter has no resemblance to the experimental spectrum either.

Note that the T_{2g} spectrum does not depend upon the parameter δf_2. More negative values of δf_s tend to shift the low-frequency peak to even lower frequencies and consequently worsen the agreement with experiment. Less negative values of δf_s, however, worsen the agreement between theory and experiment for the T_{1u} spectrum. The T_{2g} spectrum is not very sensitive to changes in δf_4 when the latter is $\simeq -\delta f_3$. Larger values of δf_4 worsen the agreement with the experimental spectrum and for $\delta f_4 \simeq \delta f_s$ the calculated spectrum has very little resemblance with the measured spectrum.

Aside from disagreements in the peak positions, which also occur in the E_g and the infrared spectra, the agreement between theory and experiment is rather good. We have discussed the discrepancies in the peak positions between experimental and calculated spectra in Ref. 1. We be-

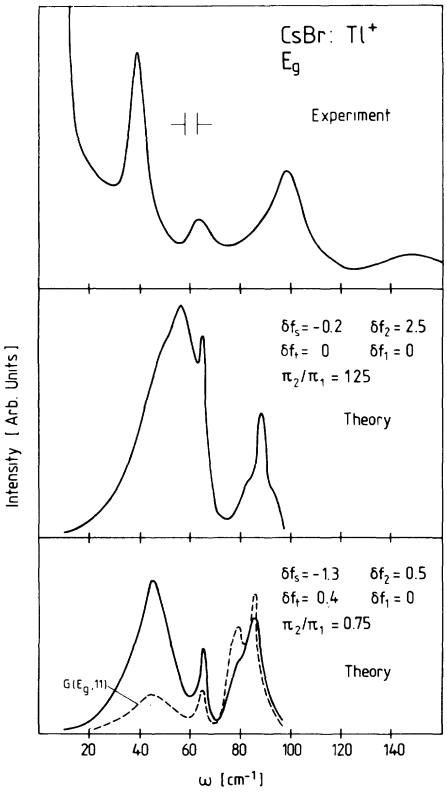

FIG. 2. Experimental and calculated E_g spectrum of CsBr:Tl⁺.

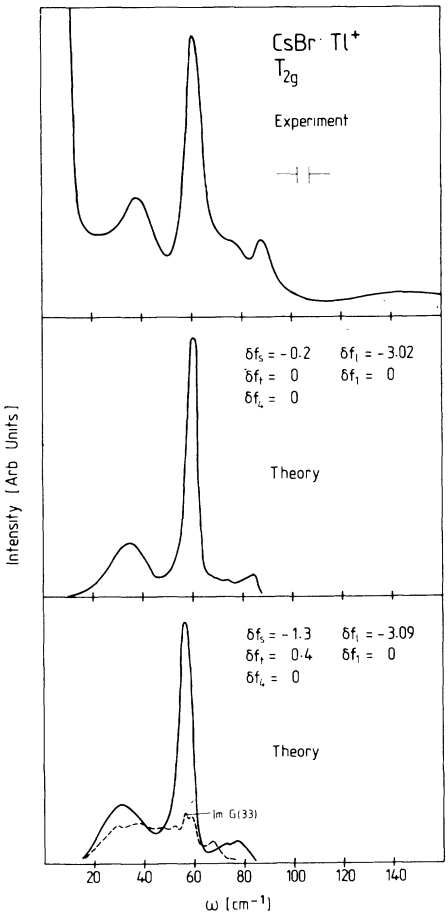

FIG. 3. Experimental and calculated T_{2g} spectrum of CsBr:Tl⁺.

lieve that these are due to inaccuracies in the calculated host-crystal phonons.

V. CONCLUSIONS

In the last section we have presented the infrared and the Raman spectra which were calculated with two different sets of perturbed BSM parameters. For the first set of parameters, to which the calculated spectra of panel 2 (Figs. 1–3) correspond, the T_{1u} and T_{2g} spectra are in excellent agreement with the corresponding experimental spectra, but the calculated E_g spectrum is very poor. For the second set of parameters, to which the calculated spectra of panel 3 of Figs. 1–3 correspond, the E_g spectrum agrees well with experiment, but the T_{1u} and T_{2g} spectra are somewhat worsened. The overall good agreement between theory and experiment for all three spectra is better when the latter set of parameters is used.

Two of the most crucial parameters in our model are δf_2 and δf_s. For crystals of Cs-halide structure a nonzero value of δf_2 is very reasonable. The value[7] that we have obtained for the other parameter, $\delta f_s = -1.3$, needs some comments.

Nonzero values of δf_s, δf_1, and δf_4 can result from two different mechanisms, namely (1) relaxation of the lattice around the defect, (2) perturbation of the electronic eigenstates on the defect's neighboring ions. For the first case, a negative value of δf_s implies on outward relaxation of the lattice (within the framework of a Born-Mayer plus Coulomb-type potential). If we now assume that only the defect's nearest neighbors are shifted to new equilibrium positions and that the force-constant changes are proportional to the relaxational displacements, then one finds $\delta f_4 \simeq -3\delta f_s = 3.9$, and $\delta f_1 \simeq \sqrt{12}\delta f_s = -4.4$, and the spectra ($T_{1u}$, E_g, and T_{2g}) calculated with these parameters are in very poor agreement with experiment. Hence, a value of $\delta f_s = -1.3$, which we have obtained from our model cannot all be an effect of lattice relaxation of the nearest neighbors. The upper limit on the values of δf_4 and δf_1 as determined from the E_g and the T_{2g} spectra are of the order 1 and -1, respectively. This would imply that the contribution from the nearest-neighbor (outward) lattice relaxation to δf_s is at the most approximately -0.3. If we now assume that there is also an outward relaxation of the second and fourth neighbors, then δf_s would become more negative and δf_4 would become smaller. This, along with the fact that the electronic eigenstates of the defect's nearest and second-nearest neighbors are perturbed by the defect, probably accounts for such a large negative value of δf_s.

We have shown in Ref. 1 that the infrared calculations do not yield information on the perturbation of the shell charge and/or that of the core-shell force constant at the defect site. Since the Raman-active modes do not involve the motion of the defect ion, these quantities remain undetermined.

Our results for the E_g spectrum clearly indicate that it is necessary to include electron-phonon interaction on the second neighbors of the defect. This is not so for the T_{2g} spectrum.

We believe that the lack of agreement in the peak positions between the experimental and the calculated spectra are primarily due to uncertainties in the calculated host-crystal phonons. In view of the fact that these were obtained by means of a fit to macroscopic parameters and not to experimentally determined dispersion of phonons (which are available only for nitrogen and room temperature[8]), such uncertainties are not unexpected.

On the basis of the results which we have obtained, we believe that a single set of perturbed BSM parameters can be used to calculate the defect-induced infrared and Raman spectra of CsBr:Tl^+, which are in reasonably good agreement with the corresponding measured spectra. Nevertheless, one very important question, which concerns the values of δY and δG, remains unanswered. As a consequence of this uncertainty, the values of perturbed parameters with which we describe our model, particulary those of δf_l and δf_t, are also uncertain. Therefore, we cannot conclude that the model which we have obtained for CsBr:Tl^+ is a unique one.

ACKNOWLEDGMENTS

We gratefully acknowledge comments by Professor U. Schröder, and we acknowledge with gratitude Dr. T. P. Martin for supplying us with his crystal.

*Present address: The University of Nebraska-Lincoln, Behlen Laboratory of Physics, Lincoln, Neb. 68588.

†Present address: Unipress High Pressure Research Center, Polish Academy of Sciences, 01-142 Warsaw, Ul. Sokolowska 29/37, Poland.

[1] M. S. Haque and D. Strauch, Phys. Rev. B 15, 5898 (1977).

[2]G. Mahler and P. Engelhardt, Phys. Status Solidi 45, 543 (1971).
[3]W. Prettl and E. Siep, Opt. Commun. 3, 407 (1971).
[4]M. Buchanan, S. Onari, and T. P. Martin, Phys. Status Solidi 70, 591 (1975).
[5]G. Mahler, Diplomarbeit (Universität Frankfurt, 1969) (unpublished).
[6]R. T. Harley, J. B. Page Jr., and C. T. Walker, Phys. Rev. B 3, 1365 (1971).
[7]Force constant values in units of e^2N/V as in Ref. 1.
[8]J. Daubert, Phys. Lett. 32A, 437 (1970); S. Rolandson and G. Raunio, Phys. Rev. B 4, 4617 (1971).